CHAPTER 5

Sol–Gel Glass and Nano–Macro Porous Bioscaffolds

MATTHIAS M. FALK,[a] TIA J. KOWAL,[a] RUI M. ALMEIDA,[b] MANAL SAAD,[c] MONA K. MAREI,[c] UKRIT THAMMA[d] AND HIMANSHU JAIN*[d]

[a] Department of Biological Sciences, Lehigh University, Bethlehem, PA, USA; [b] Departamento de Engenharia Quımica/CQE, Instituto Superior Tecnico, University of Lisbon, Lisbon, Portugal; [c] Tissue Engineering Laboratories, Faculty of Dentistry, Alexandria University, Alexandria, Egypt; [d] Department of Materials Science and Engineering, Lehigh University, Bethlehem, PA, USA
*Email: H.Jain@Lehigh.Edu

5.1 Introduction

Tissue engineering and regenerative medicine are no longer futuristic dreams[1,2] but society's realistic hope for treating patients requiring tissue or organ replacements.[3–5] In this fundamentally superior approach, a defective tissue is replaced such that a 3D scaffold structure helps the patient regenerate new natural tissue (biologic regeneration) that will last for the whole lifetime,[6] as opposed to a permanent foreign implant. The scaffold is critical to the success of this approach as it helps regenerate natural tissue and then disappears.[7] Indeed, several organs have been regenerated, and regenerative medicine is expected to grow exponentially in the future.[8] These expectations have introduced unprecedented opportunities for patients as well as challenges that need the coordinated efforts of materials scientists,

RSC Smart Materials No. 23
Bioactive Glasses: Fundamentals, Technology and Applications
Edited by Aldo R. Boccaccini, Delia S. Brauer and Leena Hupa

Published by the Royal Society of Chemistry, www.rsc.org

biologists, chemists, clinicians and engineers.[9] So far, initial success has been realized with soft tissues using polymer scaffolds,[10,11] but challenges remain for the biologic regeneration of hard tissues (bone and dental). A variety of scaffold materials and fabrication techniques has been developed for bone regeneration: ceramics, synthetic and natural polymers, metals, *etc*. Depending on the biomaterial, often unsatisfactory effectiveness in clinical repair is found because of the limited porosity, inflammatory response, mechanical instability during loading, unacceptable rates of degradation, *etc.* Nonetheless, encouraging results have been obtained with bioactive glasses (BGs) and glass-ceramics,[12] including synthetic hydroxyapatite, 45S5 Bioglass®, 55S4.3 bioactive glass, Ceravital, A-W glass ceramic, *etc.*[13–15] Overall, with properly selected composition, the glass bonds with both soft and hard tissue without the formation of an intervening fibrous layer; and it shows only minimal systemic or local toxicity, inflammation, and immunogenic response. Among BGs, the $CaO–SiO_2$ system has become the base glass for such applications to which other components may be added to meet further requirements.[16,17] The solid form of original Bioglass® 45S5, however, has been found to be of little use for hard tissue regeneration.[18,19] Interestingly, only BG has shown osteo-stimulation for bone-cell differentiation by ions leaching from the resorbing scaffolds, thus offering advantages of cellular repair at the gene level over other candidate materials.[20,21]

5.1.1 Tailored Amorphous Multi-Porous (TAMP) Bioscaffolds

The design of a bioactive scaffold is challenging because it must possess a number of highly relevant characteristics. An ideal bioscaffold for hard tissue reconstruction, for example, must satisfy the following, very diverse requirements:[17,22,23] (a) biocompatibility; (b) biodegradation at a rate that matches the tissue growth rate; (c) the leachate or dissolution products may not be harmful to the body; and (d) high porosity with interconnected 'macro' pores ($\geq$100 μm) to allow ingrowth of cells, vascularization and nutrient delivery to the new tissue. In addition, the scaffold designs should be tailored for the specific patient needs, which vary depending on their age, stature, and the type and location of the defect to be repaired. Chemical composition of the scaffold material would largely control the first three characteristics of the bioscaffold, whereas porosity is to be accomplished by using appropriate fabrication methods. The glass and glass-ceramic materials mentioned above satisfy the biocompatibility and dissolution of products requirements, and have been fabricated with suitable porosity. However, they are unacceptable in regard to degradation rate. After all, for many years glass researchers have tried improving the chemical durability of glass to last thousands of years, whereas we would like BG to degrade in weeks. An attractive solution to the challenge of increasing the degradation rate without changing the chemical composition is to increase the surface area of the bioscaffold that would be exposed to body fluids. In practice, this

can be achieved by introducing interconnected nanoporosity (~10 nm) along with much larger scale macroporosity (~100 μm).[†] The desired bioscaffold material will then have bimodal nano–macro porosity. Furthermore, it will be desirable to design this porosity to match the degradation rate and other site-specific requirements for a particular type of patient. A bioscaffold meeting all these requirements for hard tissue regeneration has been termed generally: tailored amorphous multi-porous (TAMP) material.[24]

The coexistence of nano and macro pores next to each other is thermodynamically unstable, making the fabrication of nano–macro structures a non-trivial task. On one hand, there are several approaches to introduce interconnected macroporosity in a biocompatible material, which is necessary for it to function as a scaffold for tissue regeneration. These include replication of a sponge,[25–27] 3D printing,[28] dry pressing,[29,30] freeze casting,[31] glass fiber sintering,[32] *etc*. On the other hand, there are two main approaches to introduce interconnected nanoporosity in a glass. First is the classic 'Vycor' process applicable to certain glass compositions that undergo spinodal phase separation.[33] Here a homogeneous glass prepared by the melt–quench method is heat-treated to produce spinodal decomposition into two interconnected phases. Then one phase is preferentially etched in a suitable acid, leaving behind glass with 3D porosity. In the process, the composition of the porous glass is changed from the starting composition as a part of it is leached out. The other approach is based on the sol–gel (SG) method, where the gel is comprised of a polymerized network of glass intermixed with a solution of water, alcohol and an acid or base (see Section 5.2). To obtain glass, the gel is dried and heat-treated to form a glass network (without full densification), which inevitably results in a nanoporous glass. Insofar as the liquid phase of the gel does not include any volatile component of the intended glass, the final composition should be very close to the target value.

For the above-stated reasons an SG method is preferred for making nanoporous glass bioscaffolds. To fabricate TAMP bioscaffolds then, the challenge becomes how to incorporate macroporosity—it is feasible either during the SG process or as a separate fabrication step. In this regard, note that in the conventional SG method of glass making, the nanopores are eliminated by viscous flow during sintering, as the dried gel is heated at sufficiently high temperature to obtain monolithic glass; the high surface area of nanopores serves as a strong driving force for their removal. Therefore, so long as interconnected nanoporosity is preserved, TAMP bioscaffolds can be fabricated simply by a two-step process, where nanoporous powder of desired specific surface area is prepared first by drying the gel followed by one of the various methods of introducing macroporosity mentioned above,

[†]The terms macro, meso, micro and nano porosity have different meanings in different fields. In keeping with IUPAC's basic designation we have used nanoporosity for pore size <50 nm (includes micro + meso porosity) and macroporosity for size >50 nm, although our macropores will be usually larger than 10's of microns.

such as replication of a sponge,[24,34] 3D/robotic printing,[35] dry pressing, *etc*. However, from the viewpoint of processing, a preferred method will be the one in which both nano and macro porosity are introduced in one step, *viz*. the sol–gel process. This integrated approach for fabricating TAMP bioscaffolds was introduced successfully by foaming a sol with a surfactant.[15,36] When the pore volume fraction is sufficiently large, isolated bubbles join and interconnected macroporosity is introduced in the gel. Subsequent drying of this gel produces a nano–macro porous bioscaffold as seen in Figure 5.1. Note that here the 'doorway' size is much smaller than the size of pores, and the pore volume fraction must be high (>80%) to establish connectivity between adjacent pores. As a result the mechanical strength of foamed bioscaffolds is inherently poor and the microstructure is not optimized for tissue ingrowth.[12]

Finally, a new approach based on a modified SG method was developed at Lehigh University for fabricating TAMP bioscaffolds, which focused on tailorable biodegradability by controlling the nano and macro porosity independently.[37,38] In this process, an additional spinodal phase separation ensues on the macro scale during the gelation process which produces nanoscale phase separation. Extensive *in vitro* studies show that while nanoporosity allows for control of degradation rate, additionally the cells respond more favorably than to the glass of same composition without nanoporosity. *In vitro* tests with bone forming cells and *in vivo* tests in New Zealand rabbits and dogs have shown sufficiently promising results that

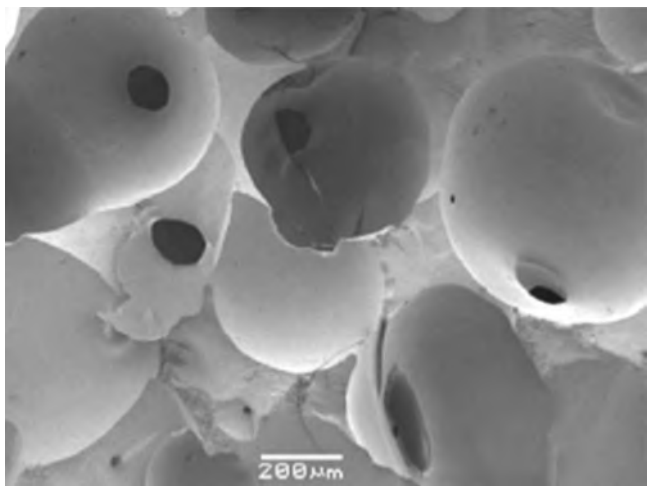

Figure 5.1 SEM micrograph showing interconnected macroporosity in 30CaO–70SiO_2 glass. Macroporosity is introduced *via* foaming of gel with a surfactant followed by sintering at 700 °C. The struts are nanoporous, so that overall the material is nano–macro porous.[15]
(Reprinted from Jones *et al.*, Optimising bioactive glass scaffolds for bone tissue engineering, *Biomaterials*, **27**, 964–973, Copyright 2006, with permission from Elsevier, ref. 15.)

a clinical trial has been initiated at the Tissue Engineering Laboratories, Alexandria University (NIH clinical trial identifier: NCT01878084). For these reasons, we believe that these nano–macro porous structures provide superior TAMP bioscaffolds for bone regeneration, especially under non-load bearing conditions. Accordingly, in this chapter we present an overview of this new process for fabricating nano–macro porous scaffolds, and key observations of performance under both *in vitro* and *in vivo* conditions. The results are discussed using the example of $30CaO–70SiO_2$ as the simple model system, although nano–macro porous glasses of more complex ternary compositions have also been prepared.[35,39]

5.2 Chemistry and Mechanisms of Fabrication of Sol–Gel Bioactive Glasses

5.2.1 Basic Concepts of Sol–Gel Processing

SG processing has emerged as a *bottom-up* technique for fabricating specialty materials.[40,41] It is used to produce a wide range of glass and ceramic materials (mainly oxides) across a large spectrum of dimensional architectures, including nanoparticles and powders, fibers, thin films, membranes, monoliths and composites. The SG process starts by the formation of a colloidal suspension (sol), its gelation and the removal of the liquid within the porous gel, which is then consolidated by heat treatment. The gelation, drying and densification steps are all critical for the control of the SG product. A basic SG process via the polymeric route may be described using the example of silica glass. Briefly, it starts with the hydrolysis of an alkoxide such as tetraethyl orthosilicate (TEOS) in the presence of a catalyst, most commonly an acid like HCl, HNO_3 or CH_3COOH but base catalysts are also employed:

$$Si(OR)_4 + nH_2O \rightarrow Si(OR)_{4-n}(OH)_n + nROH \tag{5.1}$$

with the formation of a sol. The rate of hydrolysis increases with the decrease in pH, starting from neutral solution of pH 7. Acid-catalyzed sols need longer gelling times than base-catalyzed sols, yielding gels with large volume shrinkage. By comparison, when a base such as ammonia is used as a catalyst, the gel generally shrinks less, yielding lower density products than those synthesized under acidic conditions. For silica, a pH $\sim$2–3 is required, since its isoelectric point occurs at pH $\sim$2, where the time to form a gel is the longest, rapidly decreasing for less acidic or basic conditions. Further polymerization occurs through condensation, with the formation of either water or alcohol as a by-product:

$$Si(OEt)_3OH + HOSi(OEt)_3 \rightarrow (EtO)_3SiOSi(OEt)_3 + H_2O \tag{5.2}$$

$$Si(OEt)_3OR + HOSi(OEt)_3 \rightarrow (EtO)_3SiOSi(OEt)_3 + ROH \tag{5.3}$$

The rate of condensation is also the slowest at the silica isoelectric point (pH∼2). Hydrolysis and condensation occur simultaneously, rather than sequentially. As condensation proceeds (*ageing* step), the molecules become so large that the material stiffens, with a marked increase in viscosity, and forms a gel, which may be dried subsequently and heat-treated into a dense silica glass. The overall process can be written as:

$$Si(C_2H_5O)_4 + 2H_2O = SiO_2 + 4C_2H_5OH \rightarrow \text{dry gel} \rightarrow \text{dense } SiO_2 \text{ glass} \qquad (5.4)$$

Because of the hydrophobic nature of the ethoxy groups, TEOS and water are not miscible and the presence of a co-solvent (*e.g.* an alcohol like ethanol) is necessary to attain miscibility between the reactants. The water : alkoxide ratio (R) determines the amount of co-solvent required and it controls the hydrolysis rate, together with the pH value. The stoichiometric value of R for complete hydrolysis is 4, but less water can be used since the condensation reactions may lead to water formation (eqn (5.2)).

For the synthesis of multicomponent gels, the polymeric solution route offers great possibilities. The miscibility of different alkoxide compounds allows, in principle, complete polymerization of all metal species, yielding highly homogeneous products. However, distinct rates of metal alkoxide hydrolysis may cause inhomogeneities and phase separation in the final gel. Nevertheless, if two or more different metal alkoxide precursors are used, a sequential addition procedure in which the least reactive alkoxide is pre-hydrolyzed to some extent, before the more reactive one is added, can prevent inhomogeneities from appearing. The situation becomes complicated, however, for a system like $70SiO_2$–30CaO (in mol%), when a silica precursor alkoxide like TMOS (tetramethyl orthosilicate) is pre-hydrolyzed and then mixed with calcium nitrate,[35] whose dissolution and hydration shell formation occur at a rate much faster than the hydrolysis of TMOS, so it becomes more difficult to create a truly homogeneous mixture. In this case, in fact, Fourier transform infrared (FTIR) spectroscopy indicates that the structure of the final material closely resembles that of pure silica, suggesting phase separation of the gel into silica-rich and Ca-rich phases.[42] Thus the main challenge for multicomponent gel preparation is always to control the reactivity of the more reactive precursors in order to obtain a homogeneous sol. This goal may be addressed through different strategies, namely: (1) pre-hydrolysis of less reactive compounds;[43] (2) use of complexing agents like acetylacetone;[44] (3) use of less reactive organometallic compounds like calcium acetate and triethyl orthophosphate instead of $Ca(NO_3)_2$ and P_2O_5, respectively.[37]

5.2.2 Modified Sol–Gel Process: Introduction of Multimodal Porosity *via* Multiscale Spinodal Phase Separation

The SG method produces an inherently nanoporous material initially, which starts losing porosity upon heating. Indeed, nanoporosity would persist

provided that full densification were not achieved by a prolonged heat treatment at sufficiently high temperature. Different approaches have been pursued in order to combine both nano and macro porosity in the same SG-derived glassy material: (1) Nakanishi[45] developed porous silica monoliths with a bimodal meso/macro (~0.1–40 μm) pore size distribution for high performance liquid chromatography (HPLC) column fillings. The method includes hydrolysis and polycondensation of alkoxysilanes in the presence of water-soluble polymers, which lead to polymer-induced phase separation. (2) Jones *et al.*[15,46] created interconnected macroporosity in an otherwise nanoporous phosphosilicate SG material through foaming with the help of a surfactant. The resulting material exhibits rather poor mechanical strength. (3) Marques *et al.*,[35,36,47] Vueva *et al.*,[39] Almeida *et al.*,[48] Wang *et al.*[24] and Jain *et al.*[49] developed a modified SG method to generate interconnected macroporosity combined with nanoporosity in calcium silicate and calcium phosphosilicate glasses with a coral-like morphology. Their method exploits phase separation induced by a water-soluble polymer, polyethylene oxide (PEO). (4) Maekawa *et al.*[50] produced nano/macroporous inorganic oxide monoliths with 5–10 nm nanopores and 0.1–5 μm macropores, using a polystyrene macroporous template and a self-assembling block-copolymer–SG mixture. Similarly, Wang and Jain[34] utilized the powder prepared by the SG method with polymer replication and subsequent sintering to obtain monolithic nano–macro porous samples for hard tissue regeneration, with nanopores smaller than 10 nm and macropores in the range of 300–500 μm.

Glass-in-glass phase separation is a well-known phenomenon in several modified silicate, borate and borosilicate glasses.[51] For immiscibility to occur, the separation of a liquid into two phases has to lead to a decrease in the Gibbs free energy. Depending on the initial composition, phase separation may occur by *nucleation* and *growth* of small *droplets* within a continuous glass matrix, or through a spontaneous separation into two interconnected phases by *spinodal decomposition*. The latter morphology is well suited for creating interconnected porosity when one of the phases is leached out selectively. Clearly, the choice of composition is critical for accomplishing the right kind of phase separation. In the method of Marques *et al.*,[37,38,47] spinodal phase separation is induced by a water-soluble polymer simultaneously with gelation that is catalyzed by acetic and hydrofluoric acids. The gel so produced has a polymerized skeleton separated by a liquid phase on the scale of a few nm, just as in a classical SG process. On this structure is superimposed spinodal phase separation that is created by the addition of water-soluble polymer like PEO. Removal of liquid phase from the gel made by this modified SG process leads to a coral-like interconnected morphology which includes both interconnected macropores (~10–300 μm) and nanopores (~5–50 nm),[36] as shown in Figure 5.2(a) and (b), respectively. This sample was prepared by adding appropriate quantities of TMOS and $Ca(NO_3)_2 \cdot 4H_2O$ into a solution made of PEO in acetic acid.[22] After vigorous stirring, HF was added to catalyze gelation. The sol at this stage was immediately cast into the wells of tissue culture plates.

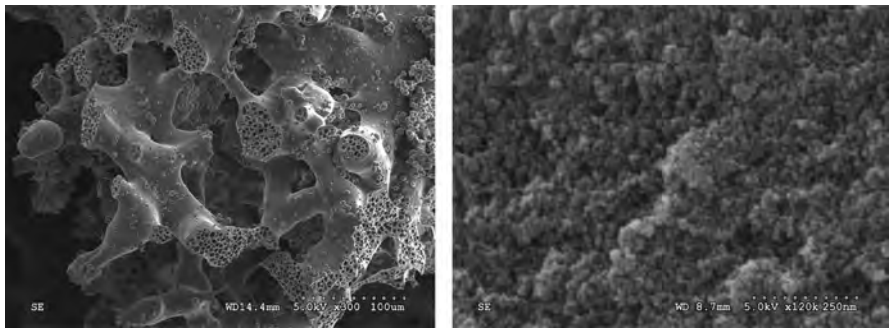

Figure 5.2 SEM micrographs of a heat-treated scaffold of composition 30CaO–70SiO_2 (mol%), prepared by the modified sol–gel process that includes PEO for creating macroscale phase separation: (a) magnification of 300× (scale bar = 100 μm); (b) magnification of 120 000× (scale bar = 250 nm). (Adapted from Marques *et al.*, *J. Mater. Res.*, 2009, ref. 38 with permission from Materials Research Society.)

Gelled samples were aged at 40 °C, and then soaked in distilled water or ammonia solution (if larger nanopores were desired) for solvent exchange before they were dried and stabilized by sintering at 700 °C. To preserve the concentration of water soluble calcium nitrate, it is important to not discard the solution but to dry it up gradually. The drying process can introduce a calcium concentration gradient locally, which may be reduced significantly during the sintering step.

Figure 5.2(a) also shows the presence of micron-sized small spheres and isolated pores which are typical of most materials prepared by this method. The composition of these microspheres is very similar to that of the matrix. Therefore, their biochemical properties should be similar to that of the surrounding scaffold. The isolated distribution of spheres and pores suggests their formation by a nucleation and growth mechanism. Apparently, they result from a droplet-like secondary phase separation together with the primary spinodal separation described above.[45] Upon drying, these droplets become micro-spheres which then dislodge from the matrix and leave behind spherical pores as seen in Figure 5.2(a).

The overall porosity exhibits a bimodal pore size distribution, with nanopores peaking at ~10 nm and macroporosity peaking around 100 μm, as shown in Figure 5.3 for a calcium phosphosilicate glass of 36CaO–$4P_2O_5$–60SiO_2 composition. The total volume fraction of porosity, determined by mercury intrusion porosimetry, is ~75%. In the modified SG method, the volume fraction of porosity, pore size and pore interconnectivity can be tailored to a large degree. On the other hand, a major challenge for the fabrication of bioactive scaffolds with interconnected macroporosity is due to the inherently poor mechanical properties when the material is used in monolithic form. This will not be a problem when the desired product is a powder or an injectable paste, for example.

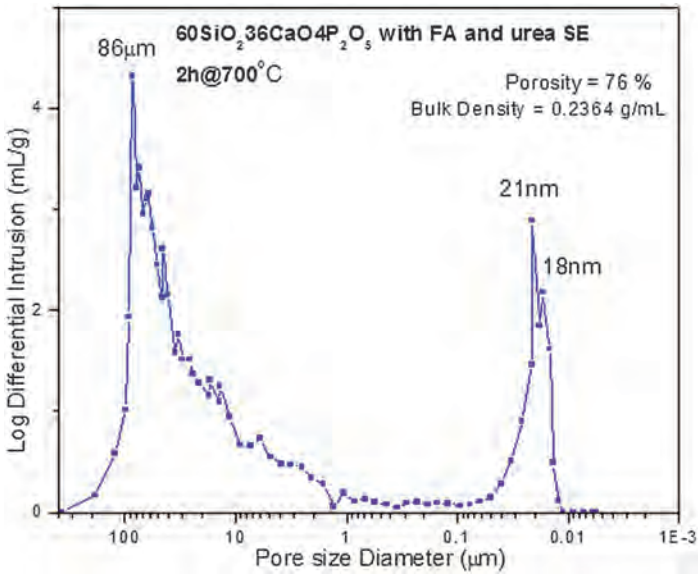

Figure 5.3 Pore size distribution in a typical nano–macro porous glass fabricated by modified sol–gel process. The data are for $36CaO–4P_2O_5–60SiO_2$ porous glass as determined using mercury porosimetry.
(Reprinted from Vueva *et al.*, *J. Am. Ceram. Soc.*, 2010, ref. 39 with permission from Wiley.)

Finally, we make note of an important chemical property of calcium silicate TAMP material. When exposed to simulated body fluid, it is readily covered with an interfacial layer of hydroxyapatite (HA, $Ca_{10}(PO_4)_6(OH)_2$)-like precipitate.[40] This mineral is known to promote the formation and bonding of bone to the substrate. Its presence is a preliminary indicator that the so-formed scaffold is biocompatible.[52,53] More detailed *in vitro* studies with bone forming cells and *in vivo* studies with animals described in Sections 5.5 and 5.6 confirm this prediction.

5.3 Biodegradation of TAMP Bioscaffolds Fabricated by Modified Sol–Gel Method

The drive behind the development of a high surface area TAMP bioscaffold was the ability to accelerate, in a controlled manner, its degradation in the body at a rate comparable to that of tissue growth. Naturally, one would like to establish how well this expectation is realized by the nano–macro porous bioactive glass, such as $30CaO–70SiO_2$ fabricated by the modified SG process described in Section 5.2.2. In this regard, we note that the basic steps of corrosion of silicate glasses in aqueous medium, such as the body fluid, which often involves both uniform dissolution and selective leaching of

certain species, are fairly well established.[54] They include ion exchange between the mobile alkali or alkaline earth cations in the glass and hydrated protons in solution, formation of a silica gel layer at the surface, dissolution of the gel layer, followed by condensation and repolymerization of the silica-rich layer. For the case of dissolution of bioactive glass in body fluids, additional reactions follow: migration of Ca^{2+} and PO_4^{3-} ions (which may be supplied by the scaffold or present in body fluid) from glass to the surface through the silica gel layer to form a layer at the top rich in CaO and P_2O_5. The calcium and phosphates in body fluid then help constitute this layer into an amorphous $CaO–P_2O_5$ layer, which then crystallizes into hydroxyl carbonate apatite (HCA). In the applications of solid bioactive glass as an implant, the HCA layer becomes the foundation of subsequent biological activities that lead to the formation of new bone on top of the glass. A strong bond between the glass and bone forms because HCA mimics the inorganic part of the natural bone. Soft tissue also bonds to bioactive glass as collagen fibrils chemisorb on the porous silica-rich layer while HCA forms on them as well as on the glass.

Although there is a reasonable understanding of the corrosion of bioactive monolithic glass implants in simulated body fluid (SBF),[52] there is very little information available on how a nano–macro porous scaffold will behave *in vivo*. Of course, the much larger surface area will enhance the corrosion rate, but we may expect significant qualitative changes as well due to the dramatic difference in diffusion through nanopores *vs*. open surface. Nucleation and growth of the HCA layer and other precipitates are also likely to be modified significantly (as seen in Figure 5.4) creating a complex degradation process.[55]

Zhang *et al.*[55] performed the first investigation of the degradation of nano–macro porous $30CaO–70SiO_2$ in SBF under quasi-dynamic conditions such that the solution was changed every day over a period of 60 days. The degradation was assessed from the dissolution of silica from the glass into

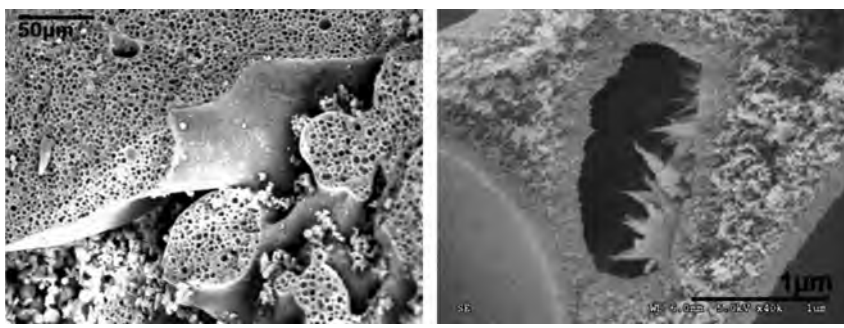

Figure 5.4 SEM micrographs of the cross-sectional surface of $30CaO–70SiO_2$ (mol%) scaffolds at 28 days in SBF. The needle-like crystals are calcium phosphate precipitates.
(Reprinted from Zhang *et al.*, *J. Am. Ceram. Soc.*, 2012, ref. 55 with permission from Wiley.)

the SBF which did not contain any silicon at the beginning, while the *in vitro* bioactivity was characterized by precipitation of calcium phosphate (CaP) on and inside the scaffold. The amount of silicon in solution was determined every day, which led to the degradation degree (DD) of the scaffold defined as percent weight of silicon in SBF solution relative to that in the original solid scaffold. In parallel, the integrity of scaffolds was followed by measuring specific surface area and pore size distribution as a function of exposure time. This study yielded the following key conclusions about the degradation of TAMP under quasi-dynamic test conditions:

1. Overall DD follows an empirical exponential law with a half-life of 15.4 days, which is a reasonable degradation rate for tissue growth. Incidentally, this trend parallels that of porous scaffolds of biodegradable polymers such as poly(D, L-lactide-*co*-glycolide).[56]
2. A closer inspection of surface area (SA) over the period of experiments indicates three mechanistic stages of the degradation process.[53] In stage I, the fluid gradually enters the scaffold over a period of about a day, indicating slow ingression into the nano–macro porous structure. During this wetting stage the sample sinks gradually as the nanopores are filled with fluid. It is characterized by an increase in solution pH due to the fast release of calcium, but little change in SA. The changes in the characteristic properties are caused mainly by the reactions, such as the precipitation of calcium phosphate, on the external surfaces of the scaffold. In stage II, the SA increases, as degradation is dominated by CaP precipitation on both the external and internal surfaces that are exposed concurrently *via* interconnected porosity. In stage III, degradation intensifies with the gradual rupturing of the structure and elimination of the nanopores as the network dissolves and CaP precipitates throughout the material. During this stage, the SA reduces and pH of the solution decreases to an almost constant level. The glass network dissolves congruently instead of calcium ion leaching; the nanopores that were exposed to the SBF gradually rupture or consolidate thus decreasing the SA. The precipitation of the CaP layer continues on the exterior, but more inside the scaffold at a higher rate as indicated by the changes in the concentration of phosphorous.
3. Although SA decreases in stage III and pore structure is modified with prolonged immersion, the overall integrity and microporous structure of the remaining scaffold are maintained throughout the immersion period. This is an important observation for the continued functioning of TAMP material as a scaffold for tissue engineering.
4. A direct relationship is found between the degradation rate and specific surface area, as seen in Figure 5.5 for two samples. Here different surface areas were obtained by using different sintering temperatures. This result demonstrates that by using appropriate processing parameters, it should be possible to tailor the degradation rate of TAMP scaffolds to match a patient's anticipated tissue regeneration rate.

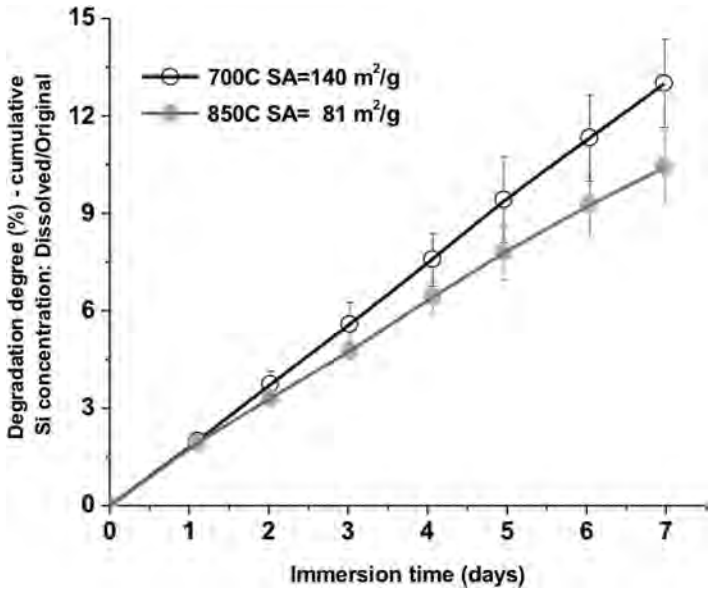

Figure 5.5 The effect of surface area (SA = 140 *vs.* 81 $m^2 g^{-1}$) on the degradation (%) of 30CaO–70SiO_2 TAMP scaffold as a function of the time of immersion in simulated body fluid (SBF). The degradation is quantified by the normalized cumulative concentration of Si dissolved in SBF for two samples sintered at 700 and 850 °C.

5.4 Cell Response to TAMP Bioscaffolds

The TAMP silicates owe hard tissue regeneration properties to their progressive dissolution in body fluids that stimulate bone cell differentiation.[57] However, the interaction between biomaterials and cells of tissues and organs is a highly complex and poorly understood process, particularly between cells and bioactive glasses. Ample research over the past years has shown that the physico-chemical characteristics of biomaterials, including bioactive glasses, such as chemical composition, surface topology, chemical reactivity, pH, charge, hydrophobicity/hydrophilicity, and dissolution behavior influence and dictate their biological performance.

We know that cells are highly capable of sensing changes in their extracellular environment including the characteristics of the surfaces to which they adhere. Cells have trans-membrane surface receptors (*e.g.* integrins) that are organized in focal adhesions and hemi-desmosomes, which are complex cellular multi-protein signaling structures that interact with specific components of natural cell substrates (the extracellular matrix, ECM) such as collagens, fibronectin, or bone-cell specific ECM-proteins (*e.g.* osteopontin, osteonectin, bone sialoprotein, *etc.*). These receptors are linked *via* actin filaments to the cell interior and allow for signaling across the cell surface membrane in both directions (inside/out signaling).[58–60]

Arginine–glycine–aspartic acid amino acid sequence motifs (Arg-Gly-Asp in the three-letter, RGD in the single letter, amino acid codes) present in extracellular matrix proteins (*e.g.* in fibronectin) are the best-known signaling motifs that are recognized by integrin receptors. It is *via* these signaling receptors that cells 'sense' their adhesive environments, and render a substrate suitable for adhesion (*e.g.* mineralized bone extracts and bioactive glasses) or unsuitable (*e.g.* titanium, polymers, Teflon® and most ceramics). Furthermore, cells react to different characteristics of adhesive substrates, with clearly detectable morphological and physiological changes.[61–65]

It is now well established that biomaterials, upon contact with protein-rich body fluids ,such as blood and lymph, instantaneously absorb proteins, which coat their surface within seconds to minutes.[66,67] Thus cells do not actually contact the biomaterial itself, but rather interact with the molecular architecture of the surface-adsorbed protein layer. Research including our own (discussed below) has shown that the mode of protein adsorption on TAMP scaffolds is directly mediated by the above-mentioned physico-chemical properties of the underlying biomaterial/scaffold.[59,64,65] Adhering cells detect protein type, protein-coat composition and protein conformation, which directly influence cellular behavior and cellular response. The scaffold morphology, composition and/or texture that may impact the cells are best investigated with cells in culture, allowing detailed microscopic and biochemical analyses of scaffold-induced cellular responses. We have primarily used MG63 human bone osteosarcoma cells (ATCC CRL-1427) and MC3T3-E1 subclone 4 mouse calvarial bone pre-osteoblasts (ATCC CRL-2593) (*i.e.* bone forming cells), which are model cell lines for bone research. Mouse osteoclasts (*i.e.* the bone degrading cells) that we isolated from mouse calvarial bone marrow, as well as epithelial and dermis cells, have also been used in our studies. MG63 and MC3T3-E1, as well as other cell types, readily adhere to both melt–quench and SG-derived TAMP bioactive glass scaffolds *in vitro*,[22,36,37,68–70] and efficiently colonize the surface as well as the inside of the scaffolds within a few days.[22] In the following sections, three examples of cellular responses to specific bioactive glass scaffold characteristics, *viz*. chemical composition, scaffold surface topology, and nanostructure, discovered in our research are described. Sections on challenges in working with highly porous bioactive glasses *in vitro* (Section 5.4.4) and on addressing future research questions follow (Section 5.6).

5.4.1 The Effect of Chemical Composition: Bioactive Glasses Substituted with Boron

Recent studies indicate that the addition of boron to bioactive glasses may further enhance bone formation.[71] Boron is an essential micronutrient acting as an ultra-trace element in concentrations <1 ppm. In plants, boron is required primarily for maintaining the integrity of cell walls while in mammals, it plays a crucial role in osteogenesis and maintenance of

bone.[72,73] Under conditions of boron deficiency, development and regeneration of bone declines.[74–76] Yet, very little is known about how this ultra-trace element exerts its beneficial health effects. Boron may interact with steroid hormones, and thus is involved in the prevention of calcium loss and bone de-mineralization.[77] Scientists began to evaluate the role of boron on the differentiation of osteoblasts and the formation of bone by adding boron to cell culture media, or Bioglass® implants. Although somewhat contradictory reports were published,[78,79] the beneficial effect of boron on osteoblast differentiation and bone formation seems compelling,[80–83] Therefore, we investigated the effect of boron by synthesizing TAMP bioactive glass scaffolds with and without a small amount of boron: normal $30CaO–70SiO_2$ and boron-substituted $30CaO–2B_2O_3–68SiO_2$ with similar structures. We found that MC3T3-E1 pre-osteoblast cells adhered significantly faster and more efficiently to boron-containing TAMP samples compared to boron-free samples. The difference became insignificant when cells grew for longer periods of time (4 and 24 hours). However, a different cellular morphology with more lamellipodial extensions, membrane ruffles and less pronounced actin stress fibers remained on boron-containing samples compared to a more roundish morphology with pronounced peripheral actin belts and pronounced stress fibers on non-boron containing TAMP samples.[84] In a related study we compared MC3T3-E1 cells on borosilicate microscopic cover glasses *vs*. on boron-free soda lime glass or tissue culture plastic substrates. The results showed a significant up-regulation of bone-specific proteins (including RunX2/Cbfa1, the master transcription factor responsible for bone-cell differentiation; bone sialoprotein 1 or osteopontin, osteocalcin, two bone-specific secreted proteins involved in matrix mineralization; collagen 1A, alkaline phosphatase, connexin 43, and three other osteoblast-relevant proteins) on boron-containing samples,[85] suggesting that doping of bioactive TAMP scaffolds with boron may further enhance their performance.

5.4.2 The Effect of Surface Topology on Attachment and Proliferation of Osteoblast Cells to Bioactive Glasses

Studies on titanium metal implants have shown that surface micro-architecture (roughness and texture) influences cell behavior.[86] However, little is known about the role of surface topology of glass on its use as an implant. In a preliminary study, Levy *et al.*[87] compared two glass samples and found greater cell proliferation on smoother samples. We systematically investigated the effect of surface roughness ($R_a \sim 0.01–1.1$ μm) on cell adhesion and proliferation on classical melt–quench prepared 45S5 Bioglass® samples *in vitro*.[67] MG63 osteosarcoma and MC3T3-E1 osteoblast precursor cells were seeded on the glass samples, and incubated for up to 6 days. The number, viability, morphology, and attachment of cells were investigated using fluorescence microscopy. The results showed that cell attachment (as indicated by cell spreading and number of focal adhesion sites) and

proliferation rate decreased with increasing roughness of the bioactive glass surface. Although these findings provide important insight for improving surface characteristics of bioactive glass bone implants, they may have less relevance for TAMP scaffolds that have an intrinsically high surface roughness from their macropores. However, sol–gel glasses prepared without macropores may benefit from these considerations.

5.4.3 The Role of Bioactive Glass Nanostructure (Nanopore Size and Phase Separation) on Cell and Protein Attachment

Nanoporosity is known to impact the performance of implants and scaffolds, such as bioactive glass (BG) scaffolds, either by providing a higher concentration of bioactive chemical species from enhanced surface area, or due to inherent nanoscale topology, or both.[20,88–92] To delineate the role of these two characteristics we fabricated bioactive glass scaffolds with nearly identical surface areas ($81–83 \pm 2$ $m^2 g^{-1}$) but significantly different nanopore sizes (av. 3.7 nm, sample F; and av. 17.7 nm, sample E) by varying both the sintering temperature and the ammonia concentration during the solvent exchange phase of the SG fabrication process (Figure 5.6A). We then performed *in vitro* tests with MC3T3-E1 pre-osteoblast cells seeded and cultured on these two types of bioactive glass scaffolds. Within 12 hours post-seeding, cells attached to the surface of both sample types and began to proliferate within 24 hours. As indicated by cellular actin–cytoskeleton staining (green), cells on all specimens exhibited a well spread epithelioid-like morphology featuring prominent stress fibers as is typical for cells adhering to stiff substrates (Figure 5.6B). However, cell density on sample F (with smaller nanopore size) was significantly higher than on sample E (with larger nanopore size) 12 hours post-seeding (Figure 5.6C). The difference in cell density on the two sample types was less pronounced by 48 hours post-seeding, although a slightly higher density of cells was detected on samples with smaller nanopore size (Figure 5.6C). No obvious differences in actin organization were observed between the two scaffold types, although higher magnification may have revealed potential structural differences. At the same time, cells do not respond to non-porous samples as well as to nanoporous surfaces (see further in Section 5.5). Taken together, these results indicate that optimized nanoporosity (in our case $\sim$4 nm compared to $\sim$18 nm diameter) can boost bioactive glass scaffold bioactivity and cell adhesion, providing clear evidence of the beneficial effect of nanopore topography in tissue engineering-relevant bioactive glass scaffolds.[68]

Interestingly, we recently obtained additional comparable results with spinodally *versus* droplet-like phase-separated 45S5 bioactive glass scaffolds that were fabricated by cooling the glass melts from different temperatures.[93] We found that MC3T3-E1 pre-osteoblast cells attached significantly faster and more efficiently to samples with spinodal morphology compared to droplet-like morphology based on cell number and morphological

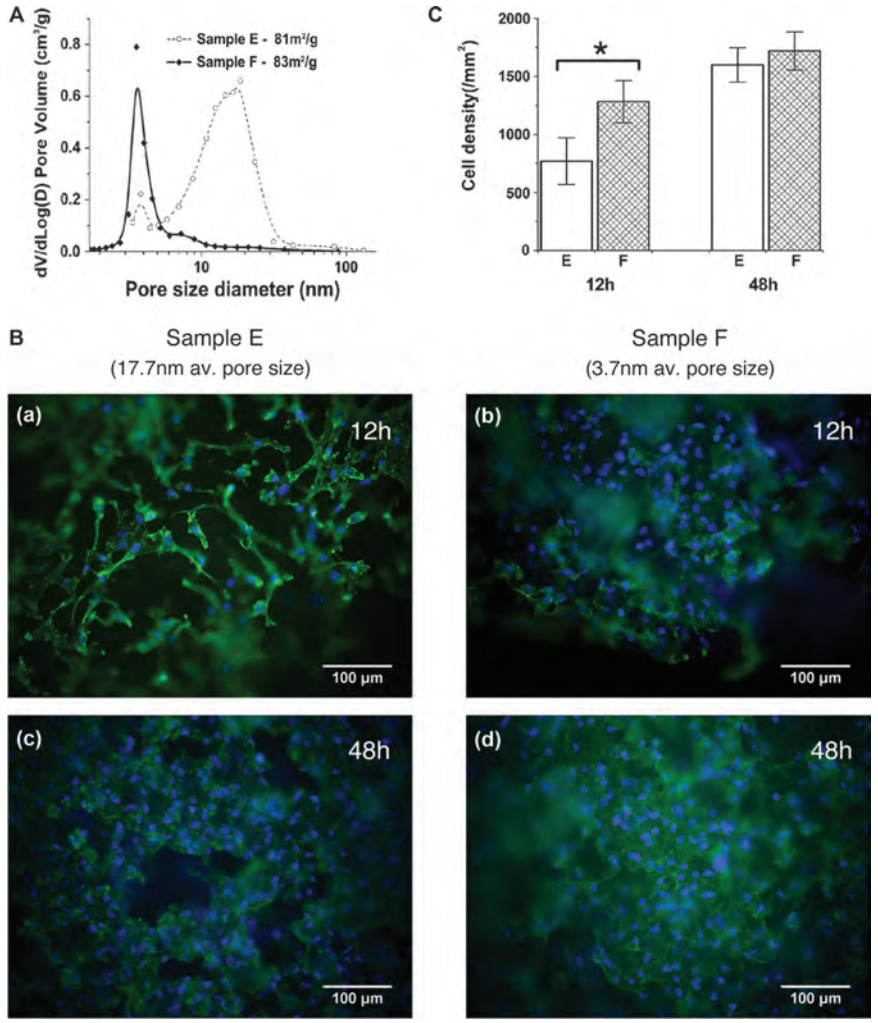

Figure 5.6 Proliferation and adhesion of bone cells on TAMP bioactive glasses with different nanoporosity. (A) Pore size distribution of samples E and F. (B) Representative micrographs of (a) samples E at 12 hours, (b) samples F at 12 hours, (c) samples E at 48 hours, and (d) samples F at 48 hours post cell seeding. MC3T3-E1 mouse calvarial bone pre-osteoblast cells were fixed with formaldehyde, F-actin was stained with Alexa 488-Phalloidin (green) to evaluate cell morphology, and cell nuclei were stained with DAPI (blue) to quantify cell density. Images were acquired using a 20× objective. (C) Cell density on samples E and F 12 and 48 hours post cell seeding. The error bars represent the standard deviation of cell density on three samples (* = statistically significant, $P < 0.05$). (Reprinted from Wang *et al.*, *Tissue Eng., Part A*, 2013, ref. 70 with permission from Mary Ann Liebert, Inc.)

characteristics. A similar result was found for bovine serum albumin (BSA), a soluble globular model protein present in abundance in the serum component of cell culture media, which attached more efficiently to the surface of spinodally phase-separated glass. Raman spectroscopy indicated a different conformational state of attached protein molecules on the two glass varieties with significantly more β-sheet and β-turn topologies on spinodally phase-separated samples.[94]

What could be the underlying mechanism that provokes such a significantly different cellular adhesion response to chemically identical substrates that differ only in structure at ~10 nm or less? Recently, the impact of nanostructure on cell functions has been studied on various material systems.[36,95–101] In these studies, introducing nanostructures, such as nano carbon/polymer fibers, or nanopores to the scaffolds enhanced cell performance. Results obtained in these studies correlate well with our *in vitro* and *in vivo* observations (see Figure 5.6 and Section 5.5). However, the precise influence of nanostructure on cell performance is still unclear and under debate. For example, Woo *et al.* suggested that incorporation of nanostructures would lead to an increased surface area, promoting protein adsorption, and hence improved cell attachment.[96] Others have suggested that nanopore topography directly influences cellular functions, either by enhancing protein adsorption,[98] changing the conformation of certain cellular attachment proteins,[102] or by changing the surface energy.[97,99] A recent *in vitro* study investigating the influence of surface characteristics of poly(methyl methacrylate) on bone formation suggests that a distinct arrangement of nanoscale disorder can stimulate mesenchymal stem cells to produce bone mineral *in vitro*, even under conditions where all other parameters (*e.g.* the size and number of nanopores, comparable to our experiments) remained unchanged,[103] supporting our findings that nanotopography determines cellular performance.

Based on these, and our own findings, we have developed the following hypothesis. Figure 5.7 represents a schematic drawn to approximate scale of the surface of nanoporous TAMP scaffolds (~4 nm on the left, ~18 nm on the right), and potential conformations of adsorbed protein that cells may encounter upon adhesion to these scaffolds. Since the chemical composition of the scaffolds is identical, proteins may absorb in similar conformations on both scaffold types (represented by the '&' symbol in scenario A). So how may a variation in pore size (the only difference) then influence cellular behavior (manifested in faster or slower cell adhesion and faster and slower initial proliferation)? One possibility (shown in A, 'Early'), for example, is that adsorbed proteins fill the small nanopores, and thus a smooth, homogenous and favorable scaffold surface is presented to cells, resulting in more efficient cell adhesion and proliferation. The larger nanopores may be too big to be filled with adsorbent proteins (*e.g.* globular albumin), generating an inhomogeneous, 'checkered' less favorable substrate surface to which cells adhere less efficiently. Adherent cells are known to secrete over time their own extracellular matrix consisting of elongated, fibrous proteins

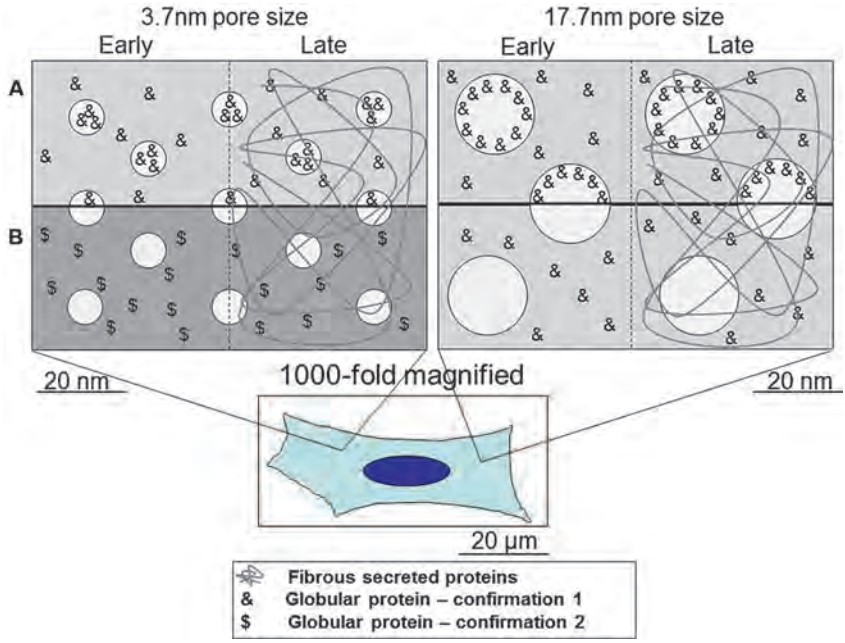

Figure 5.7 Schematic of TAMP scaffold surface topology drawn to approximate scale (2D-view; note that pores within the scaffolds are interconnected) and two hypothesized types of protein adsorption (A and B) triggering different observed cell responses (see text for further details).

(represented by crisscrossing curved lines in 'Late'). These then may also traverse and cover the larger pores transforming the scaffolds with larger pores into a similarly functioning substrate. This possibility correlates with our observation that after extended times (≥48 hours) cells grew with comparable efficiency on both scaffolds (Figure 5.6C).[36]

A second, more favorable possibility (shown in scenario B) depicts that the different physical properties of the two scaffold types cause a protein type (*e.g.* albumin) to adsorb in different conformations ('$' conformation on scaffolds with smaller nanopores, '&' conformation on scaffolds with larger nanopores). Cells prefer the protein $ conformation and thus adhere and proliferate more efficiently on the scaffolds with smaller pore size ('Early'). Later ('Late'), adsorbed proteins are again covered with cell-secreted fibrous matrix proteins and scaffold performance again becomes about equal. An earlier study, conducted on alumina, supports our second hypothesis (B), suggesting that the unfolding of the cellular adhesion protein, vitronectin, by introducing nanophase could expose an increased number of cell-adhesive epitopes that then are recognized by specific cell membrane receptors leading to enhanced cell attachment.[100] Similarly, our results investigating phase-separated 45S5 Bioglass® suggest that cell attachment to bioactive glasses is mediated by a protein layer and that the conformational state of this layer shapes cell attachment. In summary, our *in vitro* cell tests on

bioactive glass scaffolds with different nanopore size, and on phase-separated samples indicate that initial cell attachment is significantly enhanced on bioactive scaffolds with an optimum nanopore size or spinodal decomposition (a glass topology on a similar nanoscale), providing compelling evidence that nanoscale topology can significantly affect the biological performance of engineered bioactive glass scaffolds.

5.4.4 Challenges of Investigating Cells on Porous Glasses

Macroporous glasses, appearing opaque from light scattering, are unsuitable for standard light microscopic analyses that depend on transmitted light (phase-contrast, differential interference contrast (DIC), and other contrast-enhancing light microscopy techniques). Furthermore, they have a highly contoured surface topology that makes detection with high resolution, high numerical aperture (NA) oil immersion objectives challenging as some cells attached to the scaffold appear out of focus. We partially overcame these issues by staining cells with fluorescent probes (Live/Dead Viability stains, DAPI, Hoechst, Phalloidin, *etc.*) or by using antibodies directed against specific proteins (vinculin, *etc.*) that were conjugated with fluorophores (Alexa 488, Alexa 568, Rhodamine, Texas Red, Cy3, *etc.*), a technique termed indirect immunofluorescence (see Figures 5.6B and 5.8A). Acquiring images with 40× oil, and 10×, 20× and 40× air, long-distance objectives, compared to higher resolution (but narrower focal plane) 60× and 100× oil immersion objectives, also may sometimes also help generate decent images of cells growing on scaffolds that otherwise would have been beyond acquisition (see, *e.g.* Figures 5.6C and 5.8A). Figure 5.8A shows cells growing on the surface of a TAMP scaffold (detected by staining the cell nuclei with DAPI) that were imaged at two different focal planes. The image on the left shows the cells growing on the scaffold surface in focus, while the image on the right shows the cells in focus growing deep inside macroporous depressions. Scanning electron microscopy (SEM) analysis of scaffolds in general allows for adequate detection of the scaffold and overall cellular morphology in great detail (Figure 5.8B), however it does not allow observation of protein distribution inside cells. Recently, for studies that only concerned nanoporosity, we crushed TAMP samples into fine powder, which was then pressed into disks. These disk-shaped scaffolds still maintain their specific nanoporosity, but feature a much smoother surface that is far more suitable for high-resolution fluorescence light microscopic analysis.

Another challenge, especially of porous bioactive glasses, is their tremendous ability to adsorb proteins including proteins present in the serum component of cell culture media (*e.g.* albumin). Such dominant adsorption can make Western blot analyses and other biochemical assays challenging, as matrix proteins, transcription factors and other bone-cell specific marker proteins are generally expressed in much lower amounts and thus may become difficult to resolve by SDS-PAGE gels. Figure 5.8C shows a Coomassie-stained SDS-PAGE gel of MC3T3-E1 cell proteins that grew on

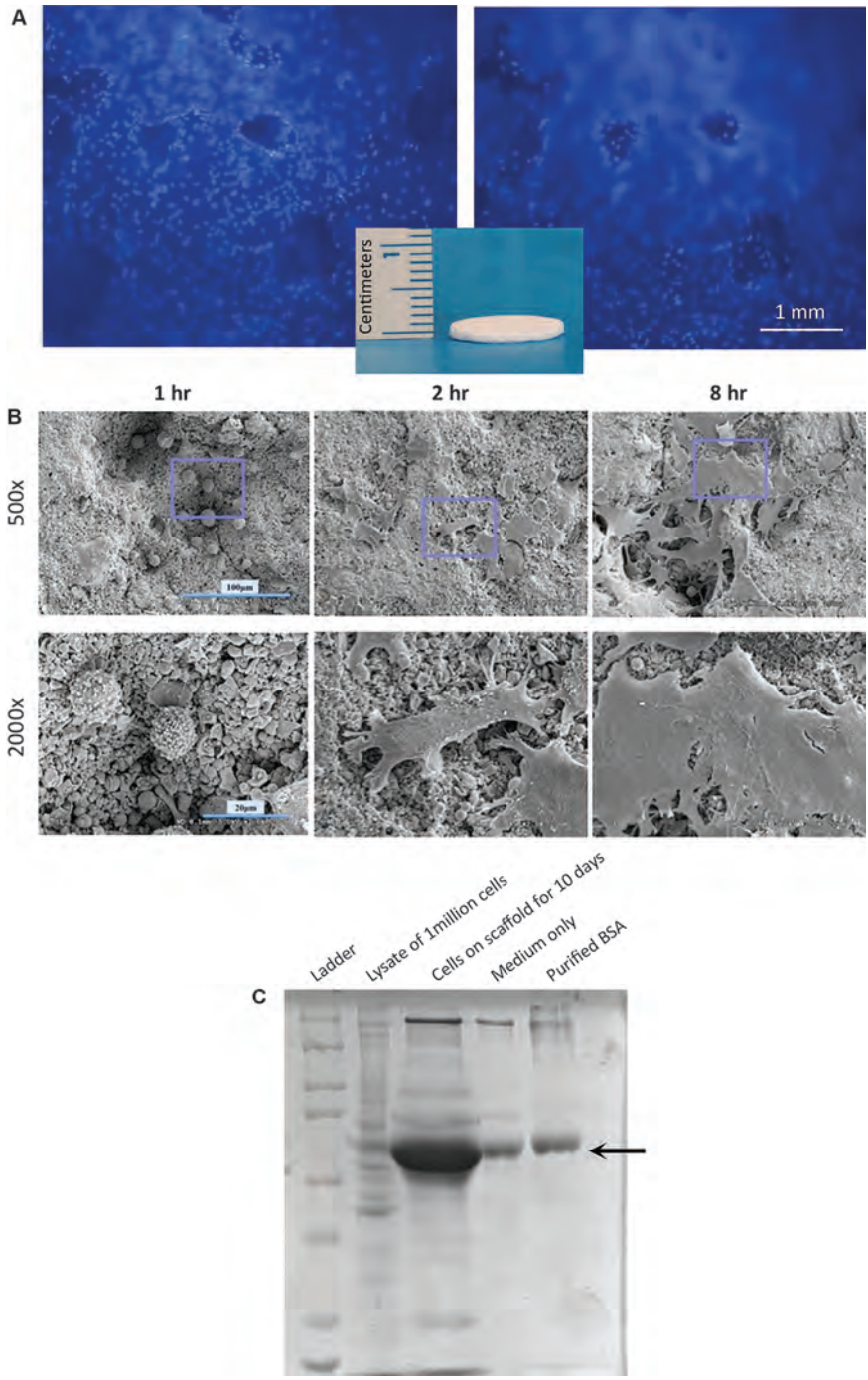
A
Centimeters
1 mm
1 hr
2 hr
8 hr
B
500x
2000x
100μm
20μm
Ladder
Lysate of 1million cells
Cells on scaffold for 10 days
Medium only
Purified BSA
C

sol–gel-fabricated TAMP scaffolds. Note the huge amount of albumin on the gel (labeled with an arrow) that totally obscured the resolution of smaller, faster-migrating cellular proteins (compare with cell lysate analyzed in the lane to the left derived from TC plastic-grown cells). We succeeded by normalizing cell lysates to a housekeeping protein that was larger than albumin (α-adaptin) and thus migrated more slowly. Consequently, its detection and quantification was not affected by the adsorbed albumin. TAMP scaffold protein adsorption can also be challenging when performing indirect immunofluorescence analyses as the secondary, fluorophore-conjugated antibodies readily adsorb to the scaffold, generating a high background fluorescence. Blocking permeabilized cell samples with large amounts of protein (5–10% bovine serum albumin or fetal calf serum) for extended times (overnight) before fluorescence analysis helped to partially overcome this issue. Quantitative cell assays may be challenging when cells have colonized inside the three-dimensional interconnected macroporosity of TAMP scaffolds, making consistent extraction of cells from the samples difficult. Crushing scaffolds into powder before adding solvent buffers has helped us perform these assays on a more quantitative basis.

Finally, a standard colorimetric assay to detect osteoblast differentiation, alizarin staining (a red stain that is based on the detection of calcified matrix as secreted by differentiated osteoblasts), cannot be performed on typical TAMP scaffolds that contain calcium. In this case, the entire scaffold is stained red, obscuring observation of cell differentiation. Overcoming these numerous, often unexpected and annoying challenges, requires more complicated analytical techniques to acquire seemingly simple results. Yet, the type of data that can be obtained (especially concerning nanostructure of scaffolds influencing cell response) makes the *in vitro* analyses of bioactive glass scaffold–cell interactions highly informative.

5.5 *In vivo* Experimental Animal Studies and Clinical Trial

A distinctive feature of TAMP bioscaffolds is the presence of interconnected nanopores that are absent in other common bioscaffolds, while interconnected macropores must exist in all bioscaffolds to facilitate tissue growth in 3D. The results in Section 5.3 and references therein have shown

Figure 5.8 Challenges of investigating cells on highly porous TAMP scaffolds. (A) Cell nuclei of MC3T3–E1 pre-osteoblasts growing on, and inside, a TAMP scaffold were stained with DAPI (blue) and imaged at low magnification in two different planes revealing the coarse surface topology of the TAMP material shown in the insert. (B) MC3T3-E1 cells growing for the indicated times on TAMP scaffolds were fixed and imaged by SEM. (C) A Coomassie-stained SDS-PAGE gel showing the large amount of albumin present in the serum component of cell culture medium that efficiently adsorbs to TAMP scaffolds (arrowed) and makes quantitative analyses, such as estimation of cell numbers, challenging.

that, by controlling nanoporosity, the biodegradation rate of a bioscaffold of a given composition can be controlled to match the tissue regeneration needs of a patient, at least under quasi-dynamic laboratory conditions. Notwithstanding, for the successful use of TAMP scaffolds in real patients, it is necessary to establish the role of nanopores under realistic testing conditions. In particular, we must establish how the larger changes in local chemistry from faster degradation of a nanoporous scaffold would affect the tissue in its vicinity? Then in view of the enhanced attachment of pre-osteoblast to TAMP substrates of specific nanopore size, as discussed in Section 5.4.3, it is important to determine whether nanoporosity may also produce a positive or negative effect on tissue response *in vivo*.

We sought to answer the above questions by performing *in vivo* experiments.[22] We implanted eight TAMP scaffolds under the skin (subcutaneously) of a New Zealand rabbit. These degraded rapidly with minimal inflammation and were replaced by normal connective tissue, as seen in Figure 5.9. Samples were harvested at different times (1, 3 and 5 weeks) and analyzed by fixation, staining (Stevenel's blue and Van Geison), and microscopic examination. Scaffolds are marked with an '*' in the figure. Only minimal inflammation (marked with yellow arrows in the 1 week image) is visible. Note how cells (stained blue) colonize the scaffolds from their edges. At three weeks, new blood vessels (marked with arrows in the 3 week image)

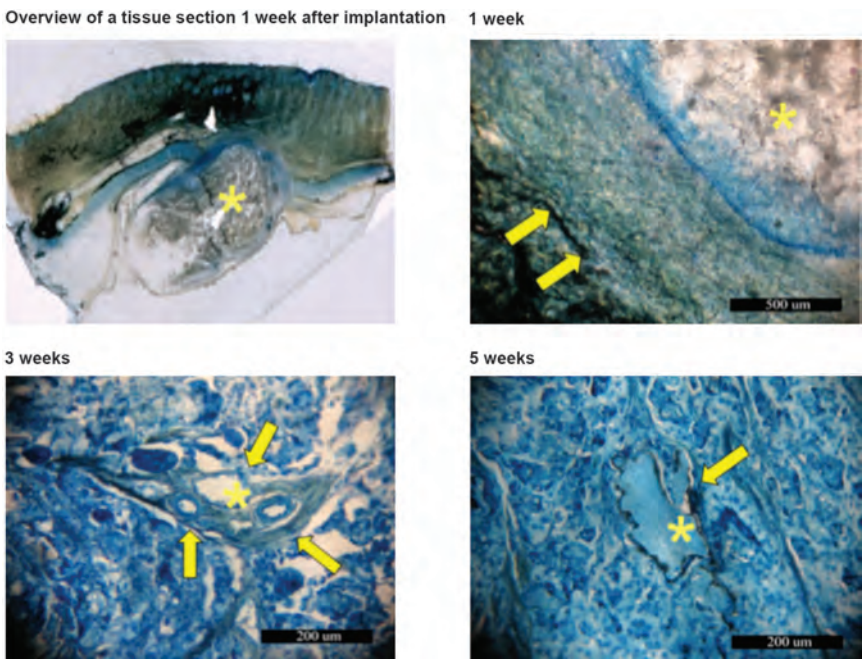

Figure 5.9 Histological analysis of TAMP scaffold and surrounding tissue after *in vivo* tests on New Zealand rabbit models for 1, 3 and 5 weeks. Scaffolds are marked with *. Top-left image shows overview at one week.

are formed in the area of the TAMP scaffold which begins to break down. At 5 weeks, only fragments of the scaffolds are left after being replaced by connective tissue with new vascularization. High cellular penetration into the scaffold is found throughout the whole region. Biodegradation of the nano–macro porous scaffold material and the observed high cellularity demonstrate the strong potential of this multi-porous material for enhancing the recruitment and proliferation of cells for new tissue formation, that gradually replace the dissolving bioactive glass. Three important conclusions are made from this study: (1) The $30CaO–70SiO_2$ TAMP scaffold is completely biocompatible. (2) It degrades *in vivo* at a rate that is comparable to the value from the laboratory test performed under quasi-dynamic conditions. Thus it will not be difficult to tailor bioscaffolds for a particular degradation rate. (3) This particular TAMP material promotes tissue regeneration of soft tissue that is similar to the surrounding tissue. Interestingly, we also found mineralized-like deposits in some samples. Evidently, this bioscaffold appears to induce regeneration of tissue appropriate for the local site, and therefore it has potential for a much broader range of applications than just hard tissue, like bone.

To establish the role of nanoporosity alone, it was important to fabricate the samples that had the same macroporosity and chemical composition, but differed only in nanoporosity. This was accomplished by preparing a nano–macro porous $30CaO–70SiO_2$ sample by sintering at 700 °C.[68] Some pieces of these samples were then further heat-treated at 840 °C, which decreased the surface area by more than an order of magnitude without altering the composition. Effectively, the latter treatment closed almost all the nanopores. These TAMP samples with and without nanopores were implanted subcutaneously in a New Zealand rabbit. The infiltration of cells, tissue formation and degradation of the scaffold were characterized at one and two weeks. At one week post implantation, cells penetrated to a depth of more than 200 μm into the macropores of the nanoporous sample, as seen in Figure 5.10. By comparison, there was no clear sign of cell penetration in the sample in which the nanopores were eliminated. At two weeks, cells also began to penetrate the macropores of the latter sample. However, the depth of penetration and the density of cells colonizing the inside of the macropores remained significantly below that observed for the former sample.

Furthermore, the nanopores seemed to enhance tissue integration with the scaffold. To reach this conclusion samples without macroporosity were implanted subcutaneously in a rabbit, with one sample having nanoporosity while another lacked any porosity.[68] Two weeks post-implantation, tissue fully integrated with the nanoporous BG scaffold, whereas the sample without nanopores consisted of unbonded interstitial regions indicative of a relatively poor scaffold integration. The origin of this difference in the tissue integration of the two types of samples can be traced to the fact that nanopores promote cell attachment as described above. As mentioned above, it is well known that cell attachment, migration, and growth are mediated by

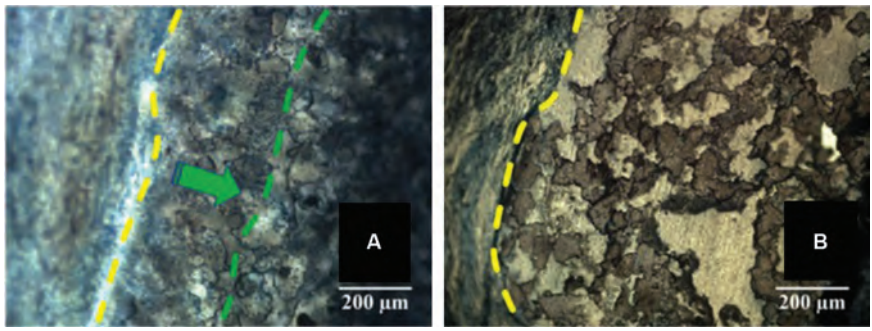

Figure 5.10 Much faster infiltration of cells in (A) nano–macro porous than in (B) macroporous-only scaffolds. Yellow and green lines represent tissue–scaffold interface at 0 and 7 days, respectively.
(Reprinted from Wang *et al.*, *Tissue Eng., Part A*, 2013, ref. 70 with permission from Mary Ann Liebert, Inc.)

proteins that absorb from serum on the surface of biomaterials.[94] Furthermore, for calcium silicates the appropriate concentration of silicate and calcium ions released from the surface can stimulate the formation and growth of bone nodules.[16] The incorporation of nanopores enhances the surface area, which, in principle, can provide an increased number of sites for protein adsorption, as well as ion concentrations optimized for more efficient cell growth. These observations and reasons strongly support the beneficial effect of nanopores incorporated into BG scaffolds, in agreement with the *in vitro* cell response to nanoporous samples discussed in Section 5.4.3.

To specifically assess the hard tissue regeneration efficacy of 30CaO–70SiO_2 TAMP material, researchers at Alexandria University evaluated *in vivo* titanium implant osseointegration in the dog mandible after using TAMP as a graft material (unpublished data). The space between the implant and socket was packed with either the TAMP powder or autogenous bone chips from the same animal, the latter serving as a reference for the TAMP test sample (see Figure 5.11). At eight weeks the tissue was harvested *en bloc* to examine the tissue regenerated around the dental implant. The results showed high osseointegration along the serrated implant surface for both kinds of powders (Figure 5.11B and C). However, the TAMP powder induced remarkably more extensive trabecular pattern and larger marrow tissue, which is attributed to the role of the bioactive glass powder that degrades rapidly due to nanoporosity. It induces angiogenesis, as demonstrated by the rich blood supply that distinguishes the cancellous bone type with its high potential of remodeling activity. This characteristic is necessary to respond to functional changes and force adaptation.

Inspired by the encouraging *in vivo* results on bone formation and osseointegration in the dog model, recently a phase I/II randomized controlled clinical trial has been initiated in humans.[104] It utilizes a split mouth technique in order to evaluate the effect of TAMP bioactive glass in bone regeneration immediately following extraction of mandibular and/or

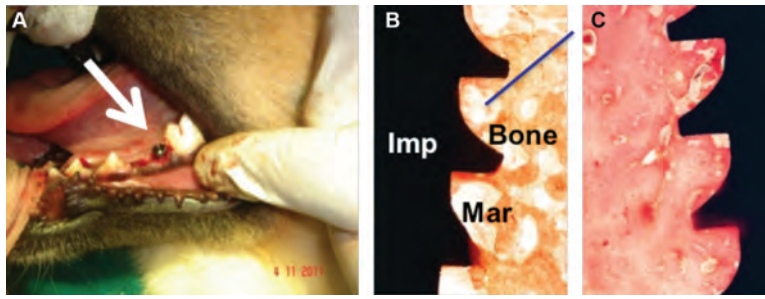

Figure 5.11 (A) Bone regeneration in canine mandible around titanium implant (Imp, shown in black) at 8 weeks. Microstructure of implant–tissue interface generated with (B) TAMP powder or (C) autogenous bone powder (40×).

maxillary premolars. Patients are followed up clinically and radiographically at 1 week, 2 weeks, and 1, 2, 3, and 6 months post-operatively. Core biopsies from the healed extraction sockets were obtained at 3 months from grafting. Preliminary histological analyses showed that the TAMP graft did not interfere with the normal healing cascade and enhanced cellularity and vascularity.

In conclusion, TAMP structures have demonstrated superior response for tissue regeneration. The results are highly promising, and provide a basis for additional required *in vivo* tests and clinical trials, before the product can be sold for use by surgeons and dentists.

5.6 Conclusions and Outlook

By exploiting a modified sol–gel preparation method, tailored amorphous multiporous bioscaffolds of calcium silicate compositions have been fabricated. The degradation rates of these materials can be optimized to suit the needs of a specific patient *via* independent control of nano and macro porosity. *In vitro* tests with cells and *in vivo* tests in animal models have established their biocompatibility and bioactivity for tissue regeneration. A clinical trial is underway to assess their potential for use in dental tissue regeneration.

In regard to the outlook for the fabrication of bioscaffolds by the modified SG route, more reproducible preparation conditions should be progressively implemented in terms of temperature and humidity control. One may also expect increasing applications involving 3D additive manufacturing and SG printing of different objects, including bioactive glass scaffolds with tailored porosity for tissue engineering and regenerative medicine.

Investigating bioactive glass–cell responses *in vitro* has revealed a large body of detailed information. Specifically, preparing TAMP bioactive glass scaffolds with small amounts of boron shed new light on the potential role of this ultra-trace element on bone cell differentiation. Future experiments

should include a careful analysis of the dissolution of boron from borosilicate and boron-containing bioactive glasses, and of mechanistic aspects that may allow cells to sense boron in solution, as well as in growth-supportive substrates. It also would seem important to test other elements such as heavy metals that may have antimicrobial or other beneficial effects.

Clearly, as our initial results have demonstrated, the nanoscale features of bioactive glass substrates, which are one thousand-fold smaller than cells themselves, have a significant impact on cellular response. The cells are able to recognize such structures of a few nanometers, which is also the size range of single integrin receptors.[105] In future many more samples with a range of nanopore size (but with the same surface area) will need to be examined to establish the optimum pore size or nanostructure for the adhesion of a specific cell type. As protein adsorption to bioactive glass scaffolds is also influenced by nanostructure, coating/impregnating scaffolds with growth factors and adhesive peptides[106] should be explored for designing 'smart' bioactive glass scaffolds.

Finally, we note that the present TAMP materials can be useful also for other biomedical applications. For instance, there is considerable current interest in biocompatible, mesoporous drug delivery systems.[107] Due to their interconnected, multi-porous structure TAMP silicates will be particularly useful for multiple drug delivery implants, which will biodegrade in a prescribed time and therefore not need removal surgery.

Acknowledgements

The multinational collaboration that made this work possible was initiated with support from the US National Science Foundation's Materials World Network (DMR-0602975) and the International Materials Institute for New Functionality in Glass (IMI-NFG, DMR-0844014) programs. This overview provides only a sampling of the literature that is available on this topic and we apologize to authors whose original works have not been cited. We thank specifically Raina H. Jain, Jutta Y. Marzillier, Shaojie Wang, and Jui Chakraborty for performing parts of the work described in Section 5.4. Work in the laboratory of MMF is supported by funds from the National Institutes of Health (NIGMS, grant GM55725).

References

1. R. Langer and J. P. Vacanti, *Science*, 1993, **260**, 920.
2. L. G. Griffith and G. Naughton, *Science*, 2002, **295**, 1009.
3. C. Constance, *Science*, 2008, **320**, 437.
4. R. F. Service, *Science*, 2008, **322**, 1460.
5. G. Naik, *The Wall Street Journal*, Front page, April 10, 2014.
6. A. Khademhosseini, R. Langer, J. Borenstein and J. P. Vacanti, *Proc. Natl. Acad. Sci.*, 2006, **103**, 2480.

7. S. J. Hollister, *Nat. Mater.*, 2005, **4**, 518.
8. G. Orlando, K. J. Wood, R. J. Stratta, J. J. Yoo, A. Atala and S. Soker, *Transplantation*, 2011, **91**, 1310.
9. V. P. Shastri and A. Lendlein, *MRS Bull.*, 2010, **35**(8), 571.
10. A. Atala, *J. Endourol.*, 2000, **14**, 49.
11. T. H. Petersen, E. A. Calle, L. Zhao, E. J. Lee, L. Gui, M. B. Raredon, K. Gavrilov, T. Yi, Z. W. Zhuang, C. Breuer and E. Herzog, *Science*, 2010, **329**, 538.
12. Q. Fu, E. Saiz, M. N. Rahaman and A. P. Tomsia, *Mater. Sci. Eng.*, 2011, **7**, 1245.
13. E. A. Kaufman, P. Ducheyne and I. M. Shapiro, *Tissue Eng.*, 2000, **6**, 19.
14. L. L. Hench, *Biomaterials*, 1998, **19**, 419.
15. J. R. Jones, L. M. Ehrenfried and L. L. Hench, *Biomaterials*, 2006, **27**, 964.
16. A. Martinez, I. Izquierdo-Barba and M. Vallet-Regi, *Chem. Mater.*, 2000, **12**, 3080.
17. P. Saravanapavan, J. R. Jones, R. S. Pryce and L. L. Hench, *J. Biomed. Mater. Res., Part A*, 2003, **66**, 110.
18. L. L. Hench, *J. Mater. Sci.: Mater. Med.*, 2006, **17**, 967.
19. J. R. Jones, P. D. Lee and L. L. Hench, *Philos. Trans. R. Soc., A*, 2006, **364**, 263.
20. L. L. Hench and J. M. Polak, *Science*, 2002, **295**, 1014.
21. L. D. K. Buttery, S. Bourne, J. D. Xynos, H. Wood, F. J. Hughes, S. P. F. Hughes, V. Episkopou and J. M. Polak, *Tissue Eng.*, 2001, **7**, 89.
22. V. Karageorgiou and D. Kaplan, *Biomaterials*, 2005, **26**, 5474.
23. Q. Z. Z. Chen, I. D. Thompson and A. R. Boccaccini, *Biomaterials*, 2006, **27**, 414.
24. S. Wang, M. M. Falk, A. Rashad, M. M. Saad, A. C. Marques, R. M. Almeida, M. K. Marei and H. Jain, *J. Mater. Sci.: Mater. Med.*, 2011, **22**, 1195.
25. H. R. Ramay and M. Q. Zhang, *Biomaterials*, 2003, **24**, 3293.
26. Q. Fu, M. N. Rahaman, B. S. Bal, R. F. Brown and D. E. Day, *Acta Biomater.*, 2008, **4**, 1854.
27. C. Vitale-Brovarone, F. Baino and E. Verne, *J. Mater. Sci.: Mater. Med.*, 2009, **20**, 643.
28. S. Michna, W. Wu and J. A. Lewis, *Biomaterials*, 2005, **26**, 5632.
29. T. Livingston, P. Ducheyne and J. Garino, *J. Biomed. Mater. Res.*, 2002, **62**, 1.
30. W. Liang, M. N. Rahaman, D. E. Day, N. W. Marion, G. C. Riley and J. J. Mao, *J. Non-Cryst. Solids*, 2008, **354**, 1690.
31. Q. Fu, M. N. Rahaman, B. S. Bal and R. F. Brown, *J. Biomed. Mater. Res., Part A*, 2010, **93**, 1380.
32. R. F. Brown, D. E. Day, T. E. Day, S. Jung, M. N. Rahaman and Q. Fu, *Acta Biomater.*, 2008, **4**, 387.
33. A. K. Varshneya, *Fundamentals of Inorganic Glasses*, Academic Press, New York, 1994, p. 66.

34. S. Wang and H. Jain, *J. Am. Ceram. Soc.*, 2010, **93**, 3002.
35. H. S. Yun, S. E. Kim, Y. T. Hyun, S. J. Heo and J. W. Shin, *Chem. Mater.*, 2007, **19**, 6363.
36. J. R. Jones and L. L. Hench, *J. Mater. Sci.*, 2003, **38**, 3783.
37. A. C. Marques, H. Jain and R. M. Almeida, *Eur. J. Glass Sci. Technol.*, 2007, **48**, 65.
38. A. C. Marques, R. M. Almeida, A. Thiema, S. J. Wang, M. M. Falk and H. Jain, *J. Mater. Res.*, 2009, **24**, 3495.
39. Y. Vueva, A. Gama, A. V. Teixeira, R. M. Almeida, S. J. Wang, M. M. Falk and H. Jain, *J. Am. Ceram. Soc.*, 2010, **93**, 1945.
40. C. J. Brinker and G. W. Scherer, *Sol-Gel Science: The Physics and Chemistry of Sol-Gel Processing*, Academic Press, NY, 1990, ch. 3, vol. 5, p. 11.
41. H. Kozuka, *Sol-gel Processing, Handbook of Sol-Gel Science and Technology*, Kluwer Academic Publishers, London, 2005, vol. 1.
42. Y. Vueva, A. Teixeira and R. M. Almeida, (unpublished results).
43. X. M. Du and R. M. Almeida, *J. Mater. Res.*, 1996, **11**, 353.
44. Y. Li and R. M. Almeida, *J. Sol-Gel Sci. Technol.*, 2012, **61**, 332.
45. K. Nakanishi, *J. Porous Mater.*, 1997, **4**, 67.
46. J. R. Jones, O. Tsigkou, E. E. Coates, M. M. Stevens, J. M. Polak and L. L. Hench, *Biomaterials*, 2007, **28**, 1653.
47. A. C. Marques, H. Jain, C. Kiely and R. M. Almeida, *J. Sol-Gel Sci. Technol.*, 2009, **51**, 42.
48. R. M. Almeida, A. Gama and Y. Vueva, *J. Sol-Gel Sci. Technol.*, 2011, **57**, 336.
49. H. Jain, A. C. Marques and R. M. Almeida, *US Pat.* 8,277,829 B2, Oct. 2, 2012.
50. H. Maekawa, J. Esquena, S. Bishop, C. Solans and B. F. Chmelka, *Adv. Mater.*, 2003, **15**, 591.
51. A. K. Varshneya, *Fundamentals of Inorganic Glasses*, The Society of Glass Technology, Sheffield, U.K., 2006, ch. 4.
52. L. L. Hench, *J. Am. Ceram. Soc.*, 1998, **81**, 1705.
53. T. Kokubo and H. Takadama, *Biomaterials*, 2006, **27**, 2907.
54. L. L. Hench, J. R. Jones and P. Sepulveda, in *Future Strategies for Tissue and Organ Replacement*, ed. J. M. Polak, L. L. Hench and P. Kemp, Imperial College Press, London, 2002, ch. 1.
55. D. Zhang, H. Jain, M. Hupa and L. Hupa, *J. Am. Ceram. Soc.*, 2012, **95**, 2687.
56. L. Wu and J. Ding, *Biomaterials*, 2004, **25**, 5821.
57. I. D. Xynos, A. J. Edgar, L. D. Butter, L. L. Hench and J. M. Polak, *Biochem. Biophys. Res. Commun.*, 2000, **276**, 461.
58. C. Kim, F. Ye and M. H. Ginsberg, *Ann. Rev. Cell Dev. Biol.*, 2011, **27**, 321.
59. N. J. Anthis and I. D. Campbell, *Trends Biochem. Sci.*, 2011, **36**, 191.
60. P. Hu and B. H. Luo, *J. Cell. Physiol.*, 2013, **228**, 306.

61. B. Geiger, J. P. Spatz and A. D. Bershadsky, *Nat. Rev. Mol. Cell Biol.*, 2009, **10**, 21.
62. E. Dejana, S. Colella, G. Conforti, M. Abbadini, M. Gaboli and P. C. Marchisio, *J. Cell Biol.*, 1988, **107**, 1215.
63. T. Yeung, P. C. Georges, L. A. Flanagan, B. Marg, M. Ortiz, M. Funaki, N. Zahir, W. Ming, V. Weaver and P. A. Janmey, *Cell Motil. Cytoskeleton*, 2005, **60**, 24.
64. A. J. Engler, S. Sen, H. L. Sweeney and D. E. Discher, *Cell*, 2006, **126**, 677.
65. D. T. Butcher, T. Alliston and V. M. Weaver, *Nat. Rev. Cancer*, 2009, **9**, 108.
66. K. Wang, C. Zhou, Y. Hong and X. Zhang, *Interface Focus*, 2012, **2**, 259.
67. K. Magyari, L. Baia, O. Popescu, S. Simon and V. Simon, *Vib. Spectrosc.*, 2012, **62**, 172.
68. H. M. M. Moawad and H. Jain, *J. Mater. Sci.: Mater. Med.*, 2009, **20**, 1409.
69. R. H. Jain, S. Wang, H. M. M. Moawad, M. M. Falk and H. Jain, in *Engineering Biomaterials for Regenerative Medicine*, ed. S. Bhatia, S. Bryant, J. A. Burdick, J. M. Karp and K. Walline, Materials Research Society, Warrendale, PA, 2010, 1235-RR03-47.
70. S. Wang, T. J. Kowal, M. K. Marei, M. M. Falk and H. Jain, *Tissue Eng., Part A*, 2013, **19**, 1632.
71. A. Hoppe, V. Mouriño and A. R. Boccaccini, *Biomater. Sci.*, 2013, **1.3**, 254.
72. D. G. Blevins and K. M. Lukaszewski, *Annu. Rev. Plant Physiol. Plant Mol. Biol.*, 1998, **49**, 481.
73. M. T. Gallardo-Williams, R. R. Maronpot, C. H. Turner, C. S. Johnson, M. W. Harris, M. J. Jayo *et al.*, *Biol. Trace Elem. Res.*, 2003, **93**, 155.
74. M. R. Naghii, G. Torkaman and M. Mofid, *Biofactors*, 2006, **28**, 195.
75. A. A. Gorustovich, T. Steimetz, F. H. Nielsen and M. B. Guglielmotti, *Anat. Rec.*, 2008, **291**, 441.
76. F. H. Nielsen, *Nutr. Rev.*, 2008, **66**, 183.
77. F. H. Nielsen, C. D. Hunt, L. M. Mullen and J. R. Hunt, *FASEB J.*, 1987, **1**, 394.
78. W. C. A. Vrouwenvelder, C. G. Groot and K. de Groot, *Biomaterials*, 1994, **15**, 97.
79. L. L. Hench, *J. Am. Ceram. Soc.*, 1991, **74**, 1487.
80. S. S. Hakki, B. S. Bozkurt and E. E. Hakki, *J. Trace Elem. Med. Biol.*, 2010, **24**, 243.
81. N. W. Marion, W. Liang, G. C. Reilly, D. E. Day, M. N. Rahaman and J. J. Mao, *Mech. Adv. Mater. Struct.*, 2005, **12**, 239.
82. A. A. Gorustovich, J. M. Porto-Lopez, M. B. Guglielmotti and R. L. Cabrini, *Biomed. Mater.*, 2006, **1**, 100.
83. R. F. Brown, M. N. Rahaman, A. B. Dwilewicz, W. Huang, D. E. Day, Y. Li *et al.*, *J. Biomed. Mater. Res., Part A*, 2009, **88**, 392.

84. J. Chakraborty, J. Y. Marzillier, T. J. Kowal, D. Zhang, H. Jain and M. M. Falk, unpublished work.
85. R. H. Jain, J. Y. Marzillier, T. J. Kowal, S. Wang, H. Jain and M. M. Falk, in *Advances in Bioceramics and Porous Ceramics IV: Ceramic Engineering & Science Proceedings*, ed. R. Narayan and P. Colombo, 2011, vol. 32, p. 111.
86. B. Boyan and Z. Schwartz, *J. Am. Acad. Orthop. Surg.*, 2006, **6**, 157.
87. S. Levy, M. V. Dalen, S. Agonafer and W. Soboyejo, *J. Mater. Sci.: Mater. Med.*, 2007, **18**, 1573.
88. D. W. Hutmacher, *Biomaterials*, 2000, **21**, 2529.
89. K. Rezwan, Q. Z. Chen, J. J. Blaker and A. R. Boccaccini, *Biomaterials*, 2006, **27**, 3413.
90. T. M. Freyman, I. V. Yannas and L. J. Gibson, *Prog. Mater. Sci.*, 2001, **46**, 273.
91. L. G. Griffith, in *Reparative Medicine: Growing Tissues and Organs*, ed. J. D. Sipe, C. A. Kelley and L. A. McNicol, New York Academy of Sciences, New York, 2002, p. 83.
92. J. R. Jones, P. D. Lee and L. L. Hench, *Philos. Trans. R. Soc., A*, 2006, **364**, 263.
93. R. Golovchak, P. Thapar, A. Ingram, D. Savytskii and H. Jain, *Acta Biomater.*, 2014, **10**, 4878.
94. R. Golovchak, T. Kowal, T. Chokshi, J. Harmes, H. Jain and M. Falk, Role of Bioglass Phase Separation in Protein and Cell Attachment, to be published.
95. K. L. Elias, R. L. Price and T. J. Webster, *Biomaterials*, 2002, **23**, 3279.
96. K. M. Woo, V. J. Chen and P. X. Ma, *J. Biomed. Mater. Res., Part A*, 2003, **67A**, 531.
97. J. Huang, S. M. Best, W. Bonfield, R. A. Brooks, N. Rushton, S. N. Jayasinghe and M. J. Edirisinghe, *J. Mater. Sci.: Mater. Med.*, 2004, **15**, 441.
98. A. L. Teixeira, P. F. Nealey and C. J. Murphy, *J. Biomed. Mater. Res., Part A*, 2004, **71A**, 369.
99. M. J. Dalby, M. J. P. Biggs, N. Gadegaard, G. Kalna, C. D. W. Wilkinson and A. S. G. Curtis, *J. Cell. Biochem.*, 2007, **100**, 326.
100. S. K. Misra, D. Mohn, T. J. Brunner, W. J. Stark, S. E. Philip, I. Roy, V. Salih, J. C. Knowles and A. R. Boccaccini, *Biomaterials*, 2008, **29**, 1750.
101. T. Raimondo, S. Puckett and T. J. Webster, *Int. J. Nanomed.*, 2010, **5**, 647.
102. T. J. Webster, L. S. Schadler, R. W. Siegel and R. Bizios, *Tissue Eng.*, 2001, **7**, 291.
103. M. J. Dalby, N. Gadegaard, R. Tare, A. Andar, M. O. Riehle, P. Herzyk, C. D. W. Wilkinson and R. O. C. Oreffo, *Nat. Mater.*, 2007, **6**, 997.

104. N. El Shazley, A. Hamdy, H. A. El-Eneen, R. M. El Backly, M. M. Saad, W. Essam, H. Moussa, M. El Tantawi, H. Jain and M. K. Marei, *JDR Clin. Trans. Res.*, 2016, DOI: 10.1177/2380084416660672.
105. M. V. Nermut, N. M. Green, P. Eason, S. S. Yamada and K. M. Yamada, *EMBO J.*, 1988, **7**, 4093.
106. C. Przybylowski, M. Ammar, C. LeBlon and S. S. Jedlicka, *J. Biomater. Nanobiotechnol.*, 2015, **6**, 146.
107. M. Vallet-Regí, F. Balas and D. Arcos, *Angew. Chem., Int. Ed*, 2007, **46**, 7548.